Research Article | Vol. 7, No. 7 | 1 Jul 2017 | OPTICAL MATERIALS EXPRESS 2424
Optical Materials EXPRESS

X-ray nanoimaging of Nd^{3+} optically active ions embedded in $Sr_{0.5}Ba_{0.5}Nb_2O_6$ nanocrystals

G. Martínez-Criado,[1,2,7] B. Alén,[3] J. A. Sans,[4] A. D. Lozano-Gorrín,[5] P. Haro-González,[6] I. R. Martín,[5] and V. Lavín[5,8]

[1]*Instituto de Ciencia de Materiales de Madrid (ICMM-CSIC), 28049 Cantoblanco, Madrid, Spain*
[2]*European Synchrotron Radiation Facility (ESRF), 38043 Grenoble, France*
[3]*IMM-CNM, Instituto de Microelectrónica de Madrid CSIC, 28760 Tres Cantos, Madrid, Spain*
[4]*Instituto de Diseño para la Fabricación y Producción Automatizada, Universitat Politècnica de València, 46022 Valencia, Spain*
[5]*Departamento de Física, MALTA Consolider Team, IMN, and IUdEA, Universidad de La Laguna, Apdo. 456, 38200 San Cristóbal de La Laguna, Santa Cruz de Tenerife, Spain*
[6]*Departamento de Física de Materiales, Universidad Autónoma de Madrid, 28049 Cantoblanco, Madrid, Spain*
[7]*gema.martinez.criado@csic.es*
[8]*vlavin@ull.edu.es*

Abstract: The spatial distribution of $Sr_{0.5}Ba_{0.5}Nb_2O_6$ nanocrystals is analyzed in a borate-based glass-ceramic by a synchrotron hard X-ray nanoimaging tool. Based on X-ray excited optical luminescence, we examined 2D projections of the Nd^{3+} optically active ions in the $Sr_{0.5}Ba_{0.5}Nb_2O_6$ nanocrystals, as well as in the glassy phase where they are embedded. Our findings reveal areas of agglomerations and/or clusters of nanocrystals ascribed to the diffusion coefficients of their constituent elements. They are characterized by high Nd^{3+} concentrations that may act as heterogeneous agents for the nucleation and growth of these nanocrystals.

OCIS codes: (160.5690) Rare-earth-doped materials; (160.5320) Photorefractive materials; (180.7460) X-ray microscopy.

References and links

1. K. Nagata, Y. Yamamoto, H. Igarashi, and K. Okazaki, "Properties of the hot-pressed strontium barium niobate ceramics," Ferroelectrics **38**(1), 853–856 (1981).
2. T. Imai, S. Yagi, H. Yamazaki, and M. Ono, "Effects of heat treatment on photorefractive sensitivity of Ce- and Eu-doped strontium barium niobate," Jpn. J. Appl. Phys. **38**(4), 1984–1988 (1999).
3. T. Volk, D. Isakov, V. Salobutin, L. Ivleva, P. Lykov, V. Ramzaev, and M. Wöhlecke, "Effects of Ni doping on properties of strontium–barium–niobate crystals," Solid State Commun. **130**(3-4), 223–226 (2004).
4. J. J. Romero, M. R. B. Andreeta, E. R. M. Andreeta, L. E. Bausá, A. C. Hernandes, and J. García-Solé, "Growth and characterization of Nd-doped SBN single crystal fibers," Appl. Phys., A Mater. Sci. Process. **78**(7), 1037–1042 (2004).
5. N. Chayapiwut, T. Honma, Y. Benino, T. Fujiwara, and T. Komatsu, "Synthesis of Sm^{3+}-doped strontium barium niobate crystals in glass by samarium atom heat processing," J. Solid State Chem. **178**(11), 3507–3513 (2005).
6. P. Haro-González, I. R. Martín, L. L. Martín, F. S. León-Luis, C. Pérez- Rodríguez, and V. Lavín, "Characterization of Er^{3+} and Nd^{3+} doped strontium barium niobate glass ceramic as temperature sensors," Opt. Mater. **33**(5), 742–745 (2011).
7. L. I. Ivleva, T. R. Volk, D. V. Isakov, V. V. Gladkii, N. M. Polozkov, and P. A. Lykov, "Growth and ferroelectric properties of Nd-doped strontium–barium niobate crystals," J. Cryst. Growth **237–239**(1), 700–702 (2002).
8. A. Marcinkevi Ius, S. Juodkazis, M. Watanabe, M. Miwa, S. Matsuo, H. Misawa, and J. Nishii, "Femtosecond laser-assisted three-dimensional microfabrication in silica," Opt. Lett. **26**(5), 277–279 (2001).
9. R. Sato, Y. Benino, T. Fujiwara, and T. Komatsu, "YAG laser- induced crystalline dot patterning in samarium tellurite glasses," J. Non-Cryst. Solids **289**(1–3), 228–232 (2001).
10. P. Haro-González, L. L. Martín, S. González-Pérez, and I. R. Martín, "Formation of Nd^{3+} doped strontium barium niobate nanocrystals by two different methods," Opt. Mater. **32**(10), 1389–1392 (2010).

#292230 https://doi.org/10.1364/OME.7.002424
Journal © 2017 Received 5 Apr 2017; revised 23 May 2017; accepted 26 May 2017; published 14 Jun 2017

Optical Materials EXPRESS

11. P. Haro-González, I. R. Martín, and A. H. Creus, "Nanocrystals distribution inside the writing lines in a glass matrix using Argon laser irradiation," Opt. Express **18**(2), 582–590 (2010).
12 B. G. Wybourne, *Spectroscopic Properties of Rare Earths* (Interscience Publishers, 1965).
13. P. Haro-González, I. R. Martín, E. Arbelo-Jorge, S. González-Pérez, J. M. Cáceres, and P. Núñez, "Laser irradiation in Nd^{3+} doped strontium barium niobate glass," J. Appl. Phys. **104**(1), 013112 (2008).
14. D. Kowalska, P. Haro-González, I. R. Martín, and J. M. Cáceres, "Analysis of the optical properties of Er^{3+}-doped strontium barium niobate nanocrystals using time-resolved laser spectroscopy," Appl. Phys., A Mater. Sci. Process. **99**(4), 771–776 (2010).
15. J. Pellicer-Porres, A. Segura, G. Martínez-Criado, U. R. Rodríguez-Mendoza, and V. Lavín, "Formation of nanostructures in Eu^{3+} doped glass-ceramics: an XAS study," J. Phys. Condens. Matter **25**(2), 025303 (2013).
16. G. Martínez-Criado, B. Alén, J. A. Sans, A. Homs, I. Kieffer, R. Tucoulou, P. Cloetens, J. Segura-Ruiz, J. Susini, J. Yoo, and G. Yi, "Spatially resolved X-ray excited optical luminescence," Nucl. Instrum. Methods Phys. Res. B **284**, 36–39 (2012).
17. G. Martínez-Criado, J. A. Sans, J. Segura-Ruiz, R. Tucoulou, A. V. Solé, A. Homs, J. Yoo, J. G.-C. Yi, and B. Alén, "X-ray excited optical luminescence imaging of InGaN nano-LEDs," Phys. Status Solidi., C Curr. Top. Solid State Phys. **9**(3–4), 628–630 (2012).
18. J. Villanova, J. Segura-Ruiz, T. Lafford, and G. Martínez-Criado, "Synchrotron microanalysis techniques applied to potential photovoltaic materials," J. Synchrotron Radiat. **19**(4), 521–524 (2012).
19. J. Smith, A. Akbari-Sharbaf, M. J. Ward, M. W. Murphy, G. Fanchini, and T.-K. Sham, "Luminescence properties of defects in nanocrystalline ZnO," J. Appl. Phys. **113**(9), 093104 (2013).
20. L. Armelao, F. Heigl, A. Jurgensen, R. I. R. Blyth, T. Regier, X.-T. Zhou, and T.-K. Sham, "X-ray excited optical luminescence studies of ZnO and Eu-doped ZnO nanostructures," J. Phys. Chem. C **111**(28), 10194–10200 (2007).
21. G. Martínez-Criado, J. Villanova, R. Tucoulou, D. Salomon, J. P. Suuronen, S. Labouré, C. Guilloud, V. Valls, R. Barrett, E. Gagliardini, Y. Dabin, R. Baker, S. Bohic, C. Cohen, and J. Morse, "ID16B: a hard X-ray nanoprobe beamline at the ESRF for nano-analysis," J. Synchrotron Radiat. **23**(1), 344–352 (2016).
22. P. B. Jamieson, S. C. Abrahams, and J. L. Bernstein, "Ferroelectric tungsten bronze-type crystal structures. I. Barium strontium niobate $Ba_{0.27}Sr_{0.75}Nb_2O_{5.78}$," J. Chem. Phys. **48**(11), 5048–5057 (1968).
23. P. Haro-González, I. R. Martín, and A. Hernández-Creus, "Nanocrystals formation on Ho^{3+} doped strontium barium niobate glass," J. Lumin. **131**(4), 657–661 (2011).
24. D. L. Griscom, in: "Borate Glasses. Structure, Properties and Applications," Plenum Press, New York, 1978, p. 11.
25. V. Lavín, U. R. Rodríguez-Mendoza, I. R. Martín, and V. D. Rodríguez, "Optical spectroscopy analysis of the Eu^{3+} ions local structure in calcium diborate glasses," J. Non-Cryst. Solids **319**(1–2), 200–216 (2003).
26. T. S. Chernaya, T. R. Volk, I. A. Verin, L. I. Ivleva, and V. I. Simonov, "Atomic structure of $(Sr_{0.5}Ba_{0.5})Nb_2O_6$ single crystals in the series of $(Sr_xBa_{1-x})Nb_2O_6$ compounds," Crystallogr. Rep. **47**(2), 213–216 (2002).
27. A. Erbil, I. I. I. Cargill III, R. Frahm, and R. F. Boehme, "Total-electron-yield current measurements for near-surface extended x-ray-absorption fine structure," Phys. Rev. B Condens. Matter **37**(5), 2450–2464 (1988).
28. V. A. Solé, E. Papillon, M. Cotte, Ph. Walter, and J. Susini, "A multiplatform code for the analysis of energy-dispersive X-ray fluorescence spectra," Spectrochim. Acta B At. Spectrosc. **62**(1), 63–68 (2007).
29. G. Martínez-Criado, A. Homs, B. Alén, J. A. Sans, J. Segura-Ruiz, A. Molina-Sánchez, J. Susini, J. Yoo, and G. C. Yi, "Probing quantum confinement within single core-multishell nanowires," Nano Lett. **12**(11), 5829–5834 (2012).
30. G. Martínez-Criado, J. Segura-Ruiz, B. Alén, J. Eymery, A. Rogalev, R. Tucoulou, and A. Homs, "Exploring single semiconductor nanowires with a multimodal hard x-ray nanoprobe," Adv. Mater. **26**(46), 7873–7879 (2014).
31. J. J. Shyu and J. R. Wang, "Crystallization and dielectric properties of SrO–BaO–Nb_2O_5–SiO_2 tungsten-bronze glass-ceramics," J. Am. Ceram. Soc. **83**(12), 3135–3140 (2000).

1. Introduction

Strontium barium niobate $Sr_xBa_{1-x}Nb_2O_6$ (SBN) crystals ($0.25 \le x \le 0.75$) belong to a family of ferroelectric materials with relevant piezo-electric, pyroelectric, and non-linear electro-optic properties [1]. Potential applications cover photorefractive memories, optical amplification, light waveguiding, lasers, temperature sensors and fibers [2–6]. The incorporation of rare earth (RE^{3+}) ions additionally produces an enhancement of its electro-optic and photorefractive coefficients [7]. As a result, the synthesis of RE^{3+}-doped SBN structures on the nanoscale has received significant attention for photonics and optoelectronics devices. In this context, one of the most promising methods is the crystallization of glasses using either laser irradiation or a conventional furnace [8,9]. The formation of $Sr_{0.5}Ba_{0.5}Nb_2O_6$ nanocrystals is triggered by a thermal treatment near the crystallization temperature of the glass. Using spatially selective cw Ar^+ laser irradiation or

Optical Materials EXPRESS

controlling the heating time of a furnace, a glass-ceramic is obtained with embedded SBN nanocrystals [5,10,11]. Owing to the ease of fabrication, the remarkable macroscopic properties and the ability to introduce RE^{3+} ions in the nanocrystals, transparent nanostructured glass-ceramics have become a unique material for optical engineering.

The incorporation of RE^{3+} ions in the SBN low-phonon energy nanocrystalline environment is paramount to increase the quantum yield of the RE^{3+} luminescence by reducing the non-radiative de-excitation rates [12]. Previous reports confirmed the inclusion of the RE^{3+} ions into the SBN nanocrystals by monitoring the emissions of Nd^{3+} at 900 nm and Er^{3+} ions at 1550 nm in the glass-ceramic compared to those of the precursor glass. About 75% of the RE^{3+} ions were incorporated in the SBN nanocrystals [13,14], probably playing the role of heterogeneous nucleating agents as in other glass-ceramics [15]. However, further studies with nanoscale spatial resolution are necessary in order to elucidate the real distribution of SBN nanocrystals. In particular, their agglomeration and/or clustering pathways could favor the non-radiative energy transfer among RE^{3+} ions, causing even quenching of the luminescence.

Although X-ray fluorescence (XRF) and diffraction (XRD) can shed light on the composition and crystal structures that coexist in the glass-ceramic (e.g. nanocrystalline and amorphous) respectively, nano-X-ray excited optical luminescence (nano-XEOL) is the only technique that makes possible the optical study of the spatial and site distributions of the RE^{3+} ions concurrently in the glass-ceramic. Based on a hard X-ray nanoprobe, this imaging tool is ideal for those applications where light emission plays the functional role. So far, XEOL has been used to investigate optical heterogeneities, defects, impurities and radiative de-excitations of optically active centers in nano-LEDS [16,17], photovoltaic materials [18], nanocrystals [19] and RE^{3+}-doped nanomaterials [20]. Unlike an UV source, which excites valence to conduction band transitions, X-ray photons excite core electrons to bound, quasi-bound or continuum states, allowing more pathways to be involved in the decay. In this work, we use nano-XEOL to analyze the distribution of SBN nanocrystals and to elucidate the role played by Nd^{3+} ions in the formation of a borate-based glass-ceramic. To our knowledge, this is the first time nano-XEOL imaging is applied to nanostructured glass-ceramics.

2. Experimental

Figure 1 shows a sketch of the experimental setup and beam profiles: a scanning XRF coupled with an XEOL setup that supplies simultaneous compositional and optical information at the nanometer scale. Developed at the hard X-ray nanoprobe end station located at 60 meters from the ESRF source (presently upgraded and relocated at 165 meters), Si mirrors mounted in crossed Kirkpatrick-Baez configuration highly focus an intense hard X-ray beam [21]. The emission of characteristic X-rays is recorded with a Si drift detector whereas the luminescence using a microscope objective lens. The latter is then focused into a multimode optical fiber and carried out of the experimental hutch to be analyzed by an optical bench consisting of a monochromator and NIR InGaAs detector.

The SBN precursor glass has a composition (in mol%) of 50 B_2O_3 – 22.5 Nb_2O_5 –11.25 SrO – 11.25 BaO – 5 Nd_2O_3. The methods of synthesis of the glass and glass-ceramic are described elsewhere [14]. XRD patterns were measured in a diffractometer (PANalytical X'Pert PRO) using the Cu $K_{\alpha 1}$ radiation. Statistical relevant XEOL data were collected in different regions of the SBN glass-ceramic monitoring the NIR emissions of the Nd^{3+} ions in the 1-1.5 eV energy range with 125 × 125 nm^2 per pixel in order to match the beam size.

Optical Materials EXPRESS

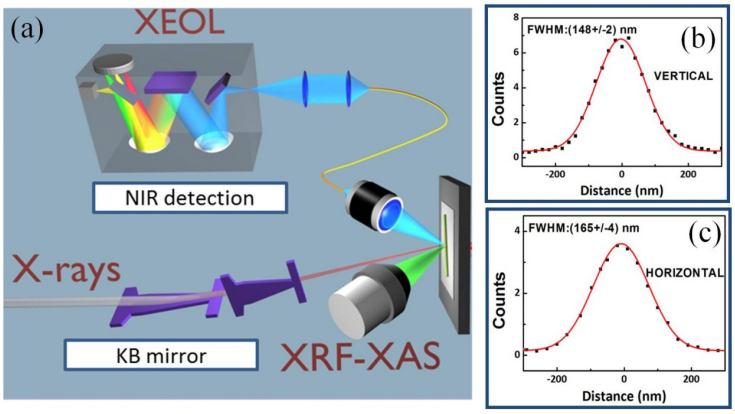

Fig. 1. (a) Schematic of the multimodal experimental setup at the hard X-ray nanoprobe beamline ID22NI (presently ID16B) at the European Synchrotron Radiation Facility. (b),(c) Focused beam profiles (vertical and horizontal) taken at 17.18 keV by means of the Au knife-edge scans.

3. Results and discussion

XRD patterns of both the precursor SBN-borate glass and the SBN glass-ceramic are compared in Fig. 2. The diffractogram of the glass shows two broad bands associated with the lack of long range order of the amorphous glass network, whereas that of the glass-ceramic also displays intense narrow peaks associated with a crystalline phase. The Rietveld refinement analysis suggests the crystalline phase to be the tetragonal tungsten–bronze structure of the $Sr_{0.5}Ba_{0.5}Nb_2O_6$ crystal [22] in the space group P4/mmm (Laue group 4/mmm), with cell parameters a = 12.4443(6) Å, b = 12.4443(6) Å, and c = 3.9010(3) Å. An average diameter of around 60 nm has been estimated for the precipitated SBN nanocrystals in this glass-ceramic using the Scherrer formula, similar to those results obtained applying AFM techniques [23].

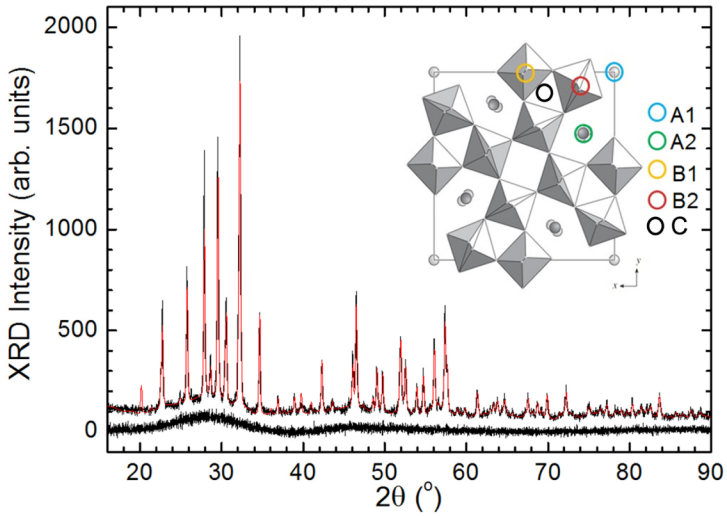

Fig. 2. XRD patterns of an SBN-borate glass (bottom) and SBN nanostructured glass-ceramic (top). Rietveld fitting of the XRD pattern for the glass-ceramic in tetragonal space group *P4/mmm* is also shown (in red). A projection of $Sr_{0.5}Ba_{0.5}Nb_2O_6$ structure onto the plane *xy* is also included, where different cationic sites are indicated.

Optical Materials EXPRESS

The glassy SBN-borate phase is composed of boron glass-former and strontium, barium and niobate glass-modifiers. The 3D network is formed by the gathering of BO_3 triangles and BO_4 tetrahedral units into well-defined borate groups [24]. The modifier cations break the borate network, and non-bridging oxygens seems to be bonded to Nd^{3+} ions in the vicinity of the breakdown, replacing the Sr^{2+} and Ba^{2+} ones with similar ionic radius. As a result, there is a large variety of environments with different distances and angles for the Nd^{3+} ions [25]. The SBN crystalline phase is a 3D network of sharing oxygen vertices of NbO_6 octahedron with three kinds of channels along the four fold axis that generate different cationic sites (see Fig. 2) [22,26]: The A_1 sites (C_4 symmetry) are partially occupied only by Sr^{2+} ions, although they also replace Ba^{2+} ions at the A_2 sites (C_S symmetry); two distorted octahedral sites, B_1 (C_{2V} symmetry) and B_2 (C_1 symmetry), are completely filled by Nb^{5+} cations with sixfold coordination; and finally, an interstitial empty C site with ninefold coordination, as well as randomly distributed oxygen vacancies. Such configuration generates a deviation from a regularly ordered structure, what is claimed to be responsible for the optical properties of the SBN crystals [22].

To obtain preliminary compositional information, XRF data were acquired with a 17.18 keV X-ray nanobeam (see Fig. 3(a)). Following the X-ray absorption events, the subsequent filling of the core holes is fulfilled by higher energy core-level electrons, causing series of radiative and non-radiative processes [27]. Part of the radiative processes give rise to XRF (K, L and M lines). Since the energies of these emissions are characteristic of individual elements, they can be used to identify the composition using *PyMca* code [28] (see Fig. 3). The XRF analysis also reveals the presence of argon due to air and other unintentional dopants or impurities, such as lead, as well as traces of palladium, gold and thulium. These unexpected elements do not seem to play a relevant role in the formation of neither the SBN nanocrystalline nor the SBN-borate glass coexisting phases. But, they may have a strong influence in the optical properties of the RE^{3+} ions acting as local optical traps. Through resonant and/or phonon-assisted energy transfer mechanisms they may produce an inhibition of the UV-Vis-NIR luminescence of the RE^{3+} ion, especially in the glassy phase.

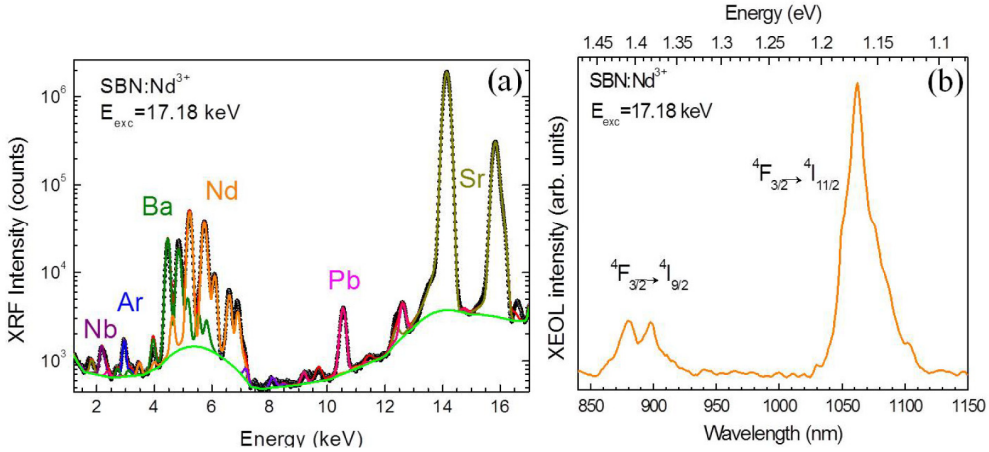

Fig. 3. (a) XRF experimental data (black dots) and fitting curves using *PyMca* code (color lines). X-ray fluorescence background (light green line) is also shown. The broad background results from the X-ray scattering by the surrounding environment (e.g., air and compact setup). (b) $^4F_{3/2}\rightarrow{}^4I_J$ (J=9/2 and 11/2) NIR XEOL luminescence of an SBN ferroelectric glass-ceramic doped with 5 mol% of Nd_2O_3 under non-selective excitation with 17.18 keV hard X-ray energy of a synchrotron radiation.

Exciting the glass-ceramic with an X-ray nanobeam of 17.18 keV, in addition to the X-ray photon absorption and XRF processes, a fraction of radiation is emitted as luminescence in the optical (UV-Vis-NIR) range. Thus, varying the beam position on the sample we can

Optical Materials EXPRESS

obtain XEOL spectra with about 150 nm spatial resolution. Figure 3(b) shows a representative XEOL spectrum, where two bands in the NIR range centered at 890 nm (1.39 eV) and 1065 nm (1.16 eV) dominate. They can be straightforwardly associated, according to the well-known Dieke's diagram, with the electric-dipole $^4F_{3/2}\rightarrow{}^4I_J$ (J = 9/2, 11/2) intra-configurational $4f^3$–$4f^3$ electronic transitions of the Nd^{3+} ions. In the glass-ceramic, Nd^{3+} ions mainly occupy the A_1 and/or A_2 sites replacing Sr^{2+} and/or Ba^{2+} with C_4 and C_S local point symmetries, respectively. Thus, the crystal-field interaction between Nd^{3+} ions and their oxygen ligands will completely break the degeneracy of the $^{2S+1}L_J$ multiplets of the free-Nd^{3+} ions giving rise to a fine structure of crystal-field, or Stark, levels [12]. Since this interaction also rules the probabilities of the absorption and emission processes of the RE^{3+} ions, the structural distortions generate small variations in the energy level scheme and in the optical properties of the Nd^{3+} ions. Accordingly, the inhomogeneous broadening of the absorption and emission bands is also affected. This effect is also suffered in a larger extent by those Nd^{3+} ions that remain in the amorphous glassy phase. Thus, the NIR emission bands would be a convolution of the emissions from the Nd^{3+} ions in the SBN nanocrystals and those remaining in the surrounding SBN-borate glass, which results in broadening profiles from both coexisting phases [13]. However, the XEOL signal seems to come mainly from those Nd^{3+} ions in the SBN nanocrystals. Two reasons may support this hypothesis: first, quantum efficiencies of the Nd^{3+} emissions in the nanocrystals are much higher and non-radiative lifetimes are longer than in the glass [10]; and second, from luminescence studies [13,14], it has been concluded that around 75% of the Nd^{3+} ions are incorporated in the SBN nanocrystals. In addition, there is another observation: the resemblance of the Nd^{3+} emissions in the glass-ceramic to those found in a pure SBN bulk crystal [4]. They also shows a structured band with two main peaks due to the emissions from the two Stark levels of the $^4F_{3/2}$ emitting multiplet to the five Stark levels of the $^4I_{9/2}$ ground state. This result suggests that the short range crystal-field interaction is practically the same in nano and bulk SBN.

The identification of the mechanisms involved in the 17.18 keV hard X-ray photon-in and the 1-1.5 eV NIR photon-out processes is not an easy task. In general terms, the XEOL process can be split into three subsequent steps: 1) core-electron excitation, 2) electron-hole thermalization and diffusion, and 3) radiative recombination. Once the X-ray absorption takes place, Auger and XRF decay processes show up to fill the core holes, producing holes at outer atomic shells and extra energy to excite electrons at shallower levels. Such secondary mechanism continues and generates electron-hole pairs in a cascade fashion till the energy is too low for further electronic excitation. In the glass-ceramic, the carriers undergo diffusion and thermalization until the electron reaches the bottom of the conduction band and the hole reaches the top of the valence band. Then, part of the energy for the electron-hole recombination has to be transferred to the Nd^{3+} ions. Thus there must be efficient non-radiative energy transfer channels to the Nd^{3+} optically active ions from those elements forming the SBN structure (Nb, Sr, Ba and O), whose energy levels are located within the forbidden band gap, or even overlapping the conduction band of the matrix. Such phenomena result into the excitation of Nd^{3+} ions to the high energy levels of the $4f^3$ ground configuration in the UV range. The Nd^{3+} ions in the UV excited levels suffer from non-radiative multiphonon and cross-relaxation de-excitation processes down to the $^4F_{3/2}$ state, from which they relax into the ^4I_J (J = 9/2, 11/2) states emitting NIR photons.

The use of the nano-XEOL technique is crucial to address the spatial distribution and formation of agglomerations or clusters, or even preferential growth areas of SBN nanocrystals in the glass-ceramic. These features affect critically the optical properties of the Nd^{3+} ions [29,30]. Black, red and green XEOL spectra shown in the upper panel of Fig. 4 represent an spatially averaged (X^{ave}) and two spatially resolved $^4F_{3/2}\rightarrow{}^4I_{11/2}$ curves taken over a representative 3 × 3 μm^2 sample area and two different spots, respectively (signals normalized for clarity: $0<X<1$). The comparison reveals spatially-dependent $^4F_{3/2}\rightarrow{}^4I_{11/2}$ emission contrasts at 1050 nm, 1060 nm and 1080 nm wavelengths. There are sample regions

Optical Materials EXPRESS

where the XEOL presents a clear double peak structure around 1050 nm, whereas in other areas these peaks merge and form a shoulder. Intensity variations at longer wavelengths are also observed with several peaks contributing to the XEOL spectrum tail around 1080 nm. Both effects are spatially correlated since higher emission intensity at the 1050 nm peak structure comes with lower emission at the long wavelength tail. Thus, these structures would play a key role and could be related to the new scheme of energy levels of the Nd^{3+} ions originated after the thermal treatment of the precursor glass with the formation of the SBN nanoparticles (i.e. it does not appear in the emission of those Nd^{3+} ions in the glassy phase).

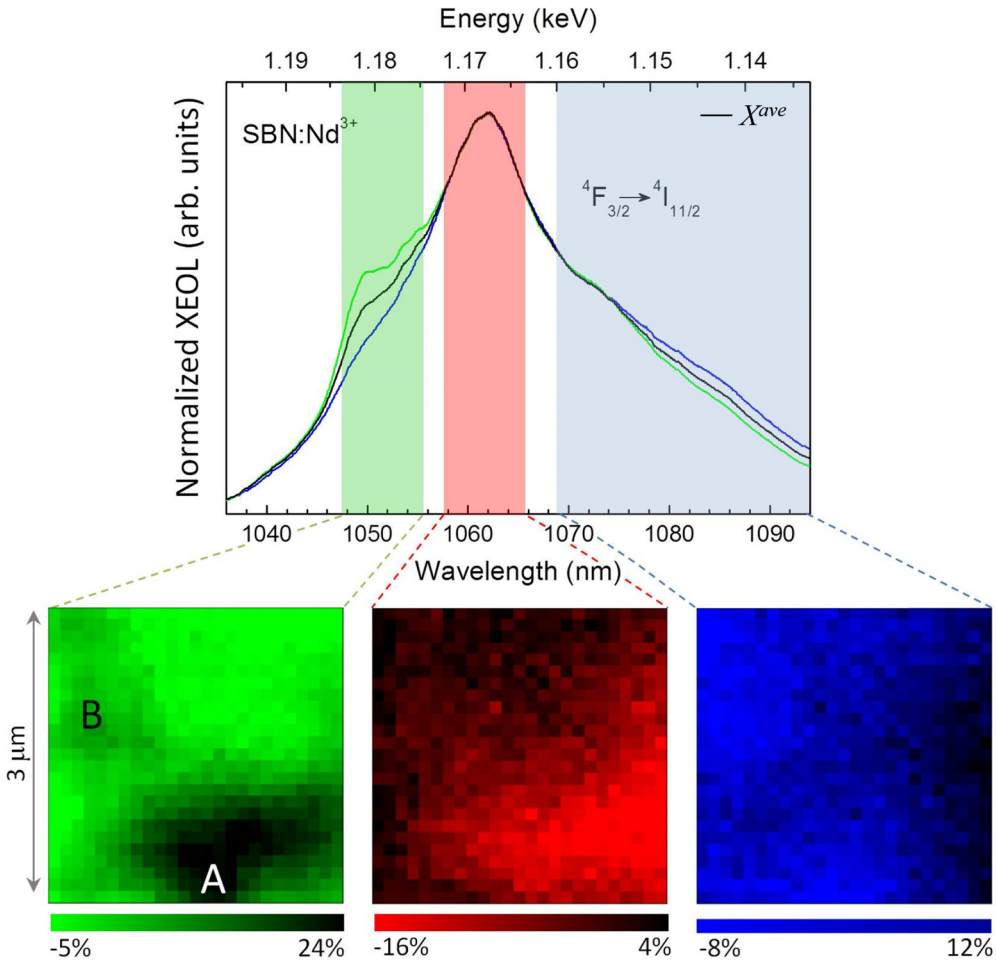

Fig. 4. $^4F_{3/2} \rightarrow {}^4I_{11/2}$ NIR XEOL spectra of an SBN ferroelectric glass-ceramic doped with 5 mol% of Nd_2O_3 under non-selective excitation with 17.18 keV hard X-ray energy of a synchrotron radiation. Maps obtained selecting different ranges of emission. They represent the relative variations of the emissions within their spectral ranges.

A further analysis can be performed by selecting different spectral ranges, Δλ (see vertical semi-transparent bands with different colors). Their corresponding maps have been generated on a pixel-by-pixel basis (i) by normalizing ($0<X_i^{\Delta\lambda}<1$) and subtracting these signals with respect to the average spectrum ($X_i^{\Delta\lambda} - X^{ave}$). Thus, the resulting relative intensity patterns (in %) show a better contrast of the Nd^{3+} luminescence, revealing spatial changes of the different channels in 2D. As a result, a picture of the distribution of Nd^{3+} ions and their site preferences, crystalline or amorphous, can be drawn for the glass-ceramic. Green and blue maps display opposite patterns in defined areas (e.g. A and B). The green pattern shows the

Optical Materials EXPRESS

luminescence of those Nd^{3+} ions mainly incorporated in the SBN nanocrystals, while the blue one exhibits the emission from Nd^{3+} mainly kept in the glassy phase. These results are confirmed by the red image, which also reveals areas of higher concentration of Nd^{3+} ions in the SBN nanocrystals associated with the existence of agglomerations or clusters of these nanoparticles in the glass-ceramic. Such spatial heterogeneity in the formation of the SBN nanocrystals, with cluster and other areas of uniform distribution well separated from the glassy phase, is confirmed by further XEOL scanning maps (not shown here). The origin is directly related to the kinetics of the nucleation and growth of SBN crystals in the borate glasses. Using laser induced crystallization techniques, the growth of crystals would be controlled by the diffusion of constituent Sr^{2+}, Ba^{2+}, Nb^{5+} and RE^{3+} ions in order to form the SBN crystals, especially the Nb^{5+} and RE^{3+} ions, which show larger diffusion coefficients [11]. Temperature gradient induced by the laser appears to be the leading driving force for the elemental redistribution of the ions in the precursor glass. For the glass, it seems reasonable to assume that almost all the Nb^{5+} ions will participate in the formation of the Nb_2O_6 network (basis of the SBN nanocrystals), competing with the B_2O_3 network for the Sr^{2+}, Ba^{2+} and Nd^{3+} ions to build their final short range order. During heating, and once the crystallization temperature is reached, the nucleation and growth of the SBN crystals are triggered. Its basic structure depends basically on the Nb^{5+} ions forming NbO_6 octahedral, with a degree of disorder imposed by the concentration of Sr^{2+}, Ba^{2+} and Nd^{3+} ions [26], reaching a volume content of about 40% [31]. This heating-induced reorder is generated by the diffusion of ions. They could be favored since the nominal composition of the Nb_2O_5–SrO–BaO compounds, easily dissolved in the B_2O_3 glass network, is the same in the precursor glass and in the SBN crystal. In fact, this '*compositional memory*' seems to play a key role in the formation of the SBN nanocrystals, although the presence of B_2O_3 affects the arrangements and diffusions of Sr^{2+}, Ba^{2+} and Nb^{5+} in such a way that induces a clearly non-uniform spatial distribution of SBN crystals. In addition, due to the large diffusion coefficients of Nb^{5+} and Nd^{3+} ions, a high concentration of the optically active Nd^{3+} ions might form part of the Nb_2O_6 tetrahedron structure, probably acting as heterogeneous seeds for the nucleation and growth of the SBN nanocrystals.

4. Summary

The formation and spatial distribution of $Sr_{0.5}Ba_{0.5}Nb_2O_6$ nanocrystals in a borate-based glass-ceramic has been successfully described based on nano-XEOL imaging. Nd^{3+} rich areas of agglomerations and/or clusters of nanocrystals were revealed and ascribed to the diffusion coefficients of their constituent elements. The Nd^{3+} ions seem to act as heterogeneous agents for the nucleation and growth of these nanocrystals.

Funding

MINECO, EU-FEDER and CSIC through the projects MAT2013-46649-C4-4-P, MAT2015-71070-REDC, MAT2016-75586-C4-2-P, MAT2016-75586-C4-4-P, 201550I021 and 201660I001, respectively.

Acknowledgments

JAS acknowledges the Spanish Program "Ramón y Cajal" for his fellowship. We also thank the ESRF for the beam time allocated and experimental facilities.